AIP | Review of Scientific Instruments

Construction and performance of a dilution-refrigerator based spectroscopic-imaging scanning tunneling microscope

U. R. Singh, M. Enayat, S. C. White, and P. Wahl

Citation: Review of Scientific Instruments **84**, 013708 (2013); doi: 10.1063/1.4788941
View online: http://dx.doi.org/10.1063/1.4788941
View Table of Contents: http://scitation.aip.org/content/aip/journal/rsi/84/1?ver=pdfcov
Published by the AIP Publishing

Construction and performance of a dilution-refrigerator based spectroscopic-imaging scanning tunneling microscope

U. R. Singh,[1,a)] M. Enayat,[1,a)] S. C. White,[1] and P. Wahl[1,2,b)]
[1]*Max-Planck-Institut für Festkörperforschung, Heisenbergstr. 1, D-70569 Stuttgart, Germany*
[2]*SUPA, School of Physics and Astronomy, University of St. Andrews, North Haugh, St. Andrews, Fife KY16 9SS, Scotland*

(Received 24 July 2012; accepted 8 January 2013; published online 30 January 2013)

We report on the set-up and performance of a dilution-refrigerator based spectroscopic imaging scanning tunneling microscope. It operates at temperatures below 10 mK and in magnetic fields up to 14T. The system allows for sample transfer and *in situ* cleavage. We present first-results demonstrating atomic resolution and the multi-gap structure of the superconducting gap of $NbSe_2$ at base temperature. To determine the energy resolution of our system we have measured a normal metal/vacuum/superconductor tunneling junction consisting of an aluminum tip on a gold sample. Our system allows for continuous measurements at base temperature on time scales of up to ≈170 h.
 [http://dx.doi.org/10.1063/1.4788941]

The properties of heavy fermion materials exhibit drastic changes under comparatively small variations in temperature, magnetic field, composition or pressure,[1] indicating a rich electronic structure in the vicinity of the Fermi level (E_F). This is reflected not only in the heavy effective mass of the conduction electrons but also in the delicate balance between localized and delocalized electronic states often found in these compounds. The relevant temperature scales for heavy fermion materials are frequently well below 1 K, therefore the experimental investigation of the changes in the electronic structure as a function of temperature and magnetic field requires very low temperatures.[2] While angle-resolved photoemission spectroscopy (ARPES),[3] the standard tool for studying electronic structure of condensed matter, has made significant progress towards the ability of measuring at temperatures below 1 K,[4] measurements in magnetic field are beyond present capabilities. In the past years, scanning tunneling spectroscopy (STS) has been shown to allow for insights into details of the band structure from spatial maps of the differential conductance. The differential conductance dI/dV is for energies close to the Fermi energy proportional to the local density of states (LDOS).[5–8] From spatial maps of dI/dV, information about electronic excitations close to the Fermi energy can be extracted, giving information on local inhomogeneities and the influence of defects.[7,9] Transforming the data into reciprocal space yields information on the dominant scattering vectors due to quasiparticle interference, revealing information about the electronic structure.[7,9,10] It has been shown that in superconducting materials, from analyzing quasiparticle interference, even the symmetry of the superconducting order parameter can be determined.[11,12] Similar studies of the superconducting order parameter in heavy fermion materials and also in organic[13] or topological[14] superconductors are highly attractive, however they require operation of the STM at temperature well below 1 K. As opposed to ARPES, where the energy resolution is a property of the analyzer, the resolution of tunneling spectroscopy is limited by the thermal broadening of the Fermi distribution of the charge carriers in the tip and is improved by going to lower temperatures.[15]

Over the past few years, a few ^{3}He-based STMs which can potentially reach temperatures down to 300 mK have been developed.[16–18] Dilution refrigerator based designs, however, which can reach temperatures well below 100 mK, are still rather rare.[19–24] Especially the set-up of UHV-compatible systems is a serious challenge, which was only recently achieved.[24] The technical difficulties in these systems are the vibrational decoupling of the pumping system, filtering of radio frequency (RF) interferences and electronic noise, and a limited choice of materials. RF filtering and shielding are very important,[25] as external RF noise can severely limit the energy resolution to an effective "electronic temperature," which is significantly higher than the nominal temperature of the experiment.

The electronic temperature of the instrument[19,20] can be determined by measuring the gap of a type-I superconductor and comparing the measured data to Bardeen-Cooper-Schrieffer (BCS) theory.[26] Typical electronic temperatures are in the range of 100–250 mK[19,20] and, in some exceptional cases, significantly lower values have been reported for STM. The lowest achieved electronic temperature of which we are aware has been reported by LeSueur and Joyez, which amounted to 45 mK electronic temperature at a measured temperature of 40 mK.[22]

In this paper, we present a dilution-refrigerator based STM optimized for the acquisition of spectroscopic maps operating at a mixing chamber temperature (T_{MXC}) below 10 mK and in magnetic fields up to 14T. The system has been optimized for high mechanical stability and continuous measurement times up to ≈170 h. The sample can be cleaved *in situ* and exchanged without the need to warm up or vent the system. We demonstrate topographic imaging with atomic

a)U. R. Singh and M. Enayat contributed equally to this work.
b)Electronic mail: gpw2@st-andrews.ac.uk.

resolution and show first spectroscopic results demonstrating an electronic temperature on the order of 140 mK.

Our millikelvin spectroscopic imaging (SI)-STM has been developed based on a dilution refrigerator with a high field magnet (0–14 T) supplied by Oxford Instruments.[27] The dilution refrigerator provides a cooling power of 400 μW at 100 mK. The design of the insert has been modified to allow for a line-of-sight port for the sample transfer. It reaches a base temperature (without the microscope head and support structure) of 7 mK at the mixing chamber as measured by a nuclear orientation thermometer. The design of our home-built STM head is based on the design by Pan.[16,28,29] Our head is optimized for high mechanical stiffness and good thermal conductivity by making the main body out of sapphire.[30] The microscope head is mounted on a copper base plate which is suspended by gold-coated copper rods from the mixing chamber plate as shown in Figs. 1(a) and 1(b) to place the STM head at the center of the magnet. The triangular walker prism is clamped between six piezo stacks[31] and hosts the scanner tube with the STM tip. The sample holder is clamped by an aluminum oxide plate to the main body. To allow for the sample transfer, the STM head is located 2 cm off-center from the main axis of the magnet (leading to a magnetic field deviating by less than 1% from the specified field[32]). The STM base plate has a number of slits to avoid eddy current heating of the base plate while ramping the magnetic field. In order to check the motion of the walker, the position can be detected by a capacitive distance sensor consisting of concentric brass cylinders.[33]

Samples can be exchanged by a vertical sample manipulator (design based on Ref. 16). For *in situ* cleavage of samples we have constructed a cleaving stage which simultaneously acts as a radiation shield when the manipulator is removed. The cleaving stage is mounted on the 4 K plate of the dilution refrigerator, the design is depicted in Fig. 2(a). The cleaver is operated by translating a rotation of the manipulator into a movement of the shutter of the cleaver, which knocks off a rod glued to the sample surface. The construction of the cleaver prevents uncleaved samples from being inserted into the STM as well as removal of the manipulator without closing the cleaver shutter.

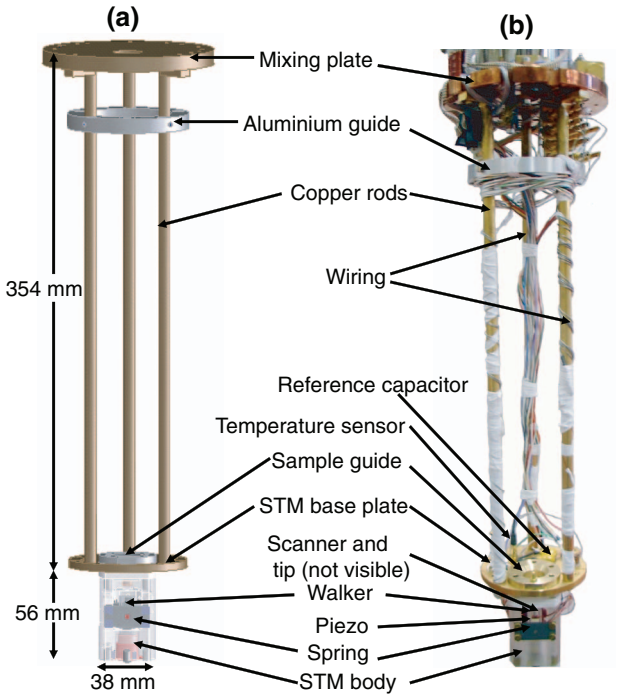

FIG. 1. Schematic view of STM assembly below the mixing chamber plate. (a) and (b) show the computer aided design model and real images, respectively.

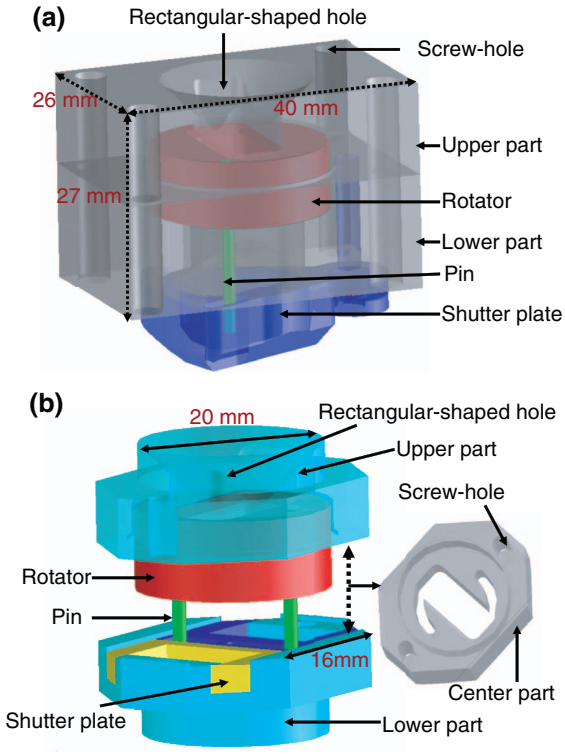

FIG. 2. (a) Sample cleaver. The sample cleaver is mounted at the 4 K-plate of the cryostat. It acts at the same time as a radiation shield to block thermal radiation from room temperature. The cleaving mechanism is operated by the sample transfer mechanism, allowing for transfer of the sample into the inner vacuum only after cleavage, (b) Shutter for thermal radiation shielding. The shutter is mounted on the still plate to block thermal radiation from the 4 K-plate from reaching the sample. The shutter is opened and closed by rotation of the manipulator similar to the cleaver.

To prevent thermal radiation along the line of sight (which, apart from the cleaver, goes from room temperature to the mixing chamber plate) from heating up the mixing chamber plate and thus the STM, an additional mechanical shutter is mounted on the still plate [Fig. 2(b)], setting its temperature to ≈600 mK. Its functional principle is similar to that of the sample cleaver, with the difference that by turning a rotational insert, two shutter plates are moved apart or towards each other. The STM head is further shielded from thermal radiation by a cylinder attached to an intermediate cold plate (at ∼50 mK) to block thermal radiation from the inner vacuum cane which is at 4 K.

Due to the extreme sensitivity of the tunneling current to the tip-sample distance, the cryostat is mounted on a vibration-isolation table suspended on air springs.[34] All pumping lines run through vibration isolation consisting of wooden boxes filled with sand, the still line is additionally

decoupled by two bellows. All gas lines and pumping tubes are clamped to the vibration table prior to their connection to the insert.

Environmental RF noise can perturb the tunnel current thus increasing the effective temperature of the STM. All electric lines entering the insert except for the tunnel current go through RF filters at room temperature, which are effective in a frequency range from 10 MHz to 10 GHz.[35] The temperature of the mixing chamber is below 10 mK and the temperature of the STM head is below 30 mK (T_{STM}) as measured by calibrated RuO_2 sensors.[36]

The STM head is controlled by a commercial digital signal processor controller built by Soft DB[37] with the open source scanning probe microscopy control software GXSM[38,39] and both home-built high-voltage amplifier and piezo motor controller. As a current amplifier, we use a commercial variable gain amplifier.[40]

We have carried out SI-STM measurements on a $NbSe_2$ single crystal at the base temperature $T_{MXC} \approx 10$ mK. We have used a mechanically cut Pt-Ir wire for the tip and cleaned it *in situ* by field emission on a gold single crystal at voltages up to 180 V applied between the tip and sample. Figure 3(a) shows a topographic image of an $NbSe_2$ surface, revealing atomic resolution as well as the known charge density wave order.[41] From the line cut profile in Fig. 3(b), the vertical stability of the instrument can be estimated to be better than 15 pm.

For the spectroscopy we measure the tunneling spectra under open feedback loop conditions. The dI/dV signal is measured using a lock-in amplifier. In Fig. 3(c) we present the spatially averaged spectra of ~6000 differential conductance spectra taken over a large area spectroscopic map showing two different gap values. We have determined them by fitting the sum of two Dynes gap equations:[43]

$$\frac{dI}{dV}(V) = \sum_{n=1,2} C_n \left| \mathrm{Re}\left[\frac{eV - i\Gamma_n}{\sqrt{(eV - i\Gamma_n)^2 - \Delta_n^2}} \right] \right| + D, \quad (1)$$

where V is the bias voltage and $\frac{dI}{dV}(V)$ the differential conductance (neglecting thermal broadening and assuming a constant tip density of states for the tip). Γ_n and Δ_n denote the quasiparticle-lifetime broadening and size for each of the two gaps. C_n are constant prefactors and D is an overall constant background. We have found the size of the large gap $\Delta_1 \approx 1.2$ meV and of the small gap $\Delta_2 \approx 0.4$ meV, comparable to previous reports.[44]

To determine the energy resolution of our dilution-refrigerator based SI-STM, we have performed measurements on a superconductor-vacuum-metal junction, using a piece of aluminum wire as material for the STM tip and a Au(111) crystal as a sample.[45] Aluminum is a conventional superconductor described well by BCS theory and has a critical temperature $T_c \simeq 1.2$ K.[19] The aluminum tip has been cleaned *in situ* by field emission as described above. Measurements have been carried out at $T_{MXC} \approx 10$ mK. We apply a modulation in the range of 5–50 μV to the sample.

We have modeled our spectra following Bardeen's theory of tunneling,[46] accounting for thermal broadening due to the Fermi distribution and lock-in broadening.[47] With the assumptions of a constant tip-sample separation and constant sample DOS in the energy range of interest, the tunneling conductance can be expressed as

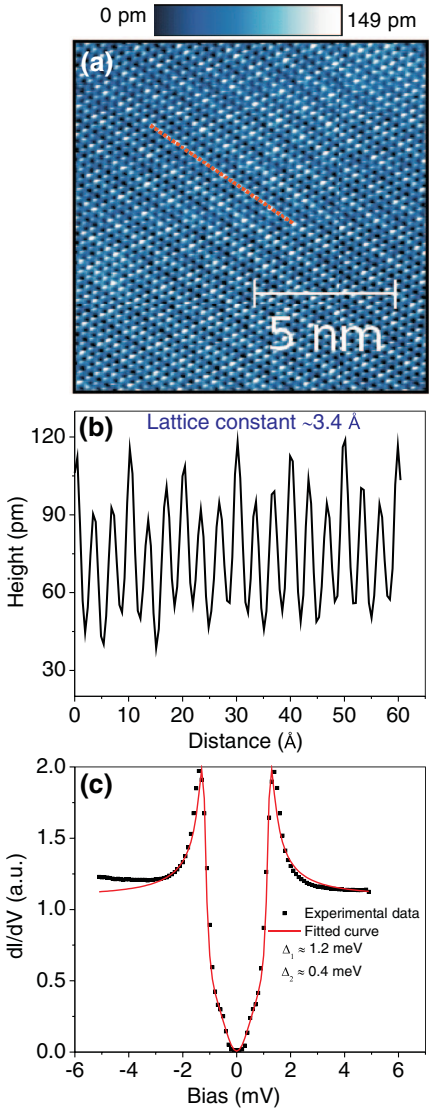

FIG. 3. (a) Atomically resolved topography of a cleaved $NbSe_2$ surface (12 × 12 nm^2, $V = 90$ mV, and $I = 0.5$ nA) measured at $T_{MXC} \approx 10$ mK. Besides the surface atomic structure, a modulation due to formation of a charge density wave can be seen. (b) Line cut along an atomic row, it can be seen that the residual noise is below 15 pm.[42] (c) Spatially averaged spectra taken on $NbSe_2$ (spectroscopy set-point: $V = 90$ mV, $I = 1$ nA, lock-in modulation of 100μV, and frequency of 511 Hz) at base temperature, the solid line shows a fit of Eq. (1) to the data.

$$\frac{dI}{dV}(V) \propto \int_{-\infty}^{\infty} \rho_{Al}(E) \times \left[\frac{-\partial f(E + eV)}{\partial V} \right] dE, \quad (2)$$

where $\rho_{Al}(E)$ represents the DOS of the superconducting aluminium tip and $f(E)$ is the Fermi-Dirac distribution in the sample. The BCS gap equation for $\rho_{Al}(E)$ is

$$\rho_{Al}(E) \propto \begin{cases} \frac{|E|}{\sqrt{E^2 - \Delta^2}} & [|E| \geq \Delta] \\ 0 & [|E| \leq \Delta] \end{cases} \quad (3)$$

with Δ being the size of the superconducting gap. The broadening due to the lock-in modulation V_{RMS} is accounted for

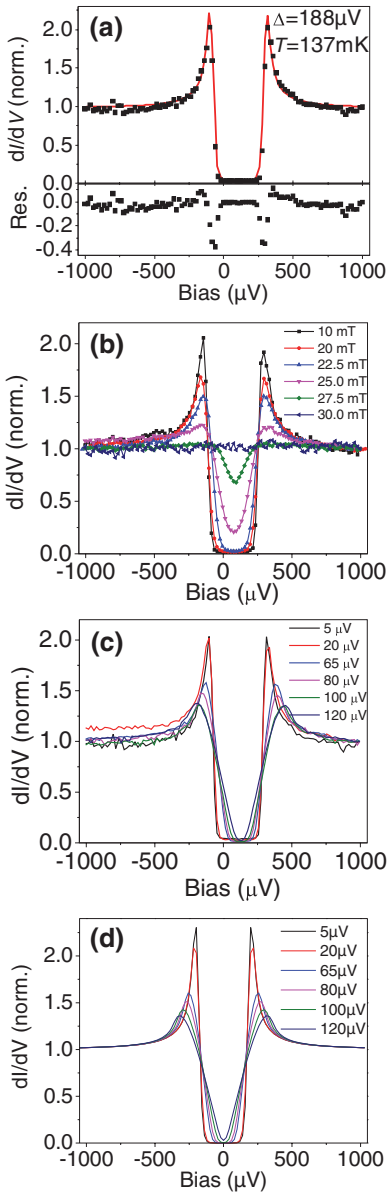

FIG. 4. Tunneling spectroscopy of a gold-vacuum-aluminum-junction at $T_{MXC} \approx 10$ mK with $V = 2$ mV and $I = 3$ nA (a) Fit of Eq. (4) to a spectrum of the Au-vacuum-Al junction for a lock-in modulation of 5 μV, yielding an electronic temperature of ≈140 mK. (b) Tunneling spectroscopy as a function of applied magnetic field. The superconducting gap disappears at magnetic fields on the order of 30 mT. (c) and (d) Tunneling and calculated spectra as a function of lock-in modulation (frequency: 511 Hz).

from the convolution of Eq. (2) with a half-circle,

$$G_{fit}(V) \propto \int_{-\sqrt{2}V_{ac}}^{\sqrt{2}V_{ac}} \frac{dI}{dV}(V+E)\sqrt{2V_{ac}^2 - E^2}dE. \qquad (4)$$

The calculated spectrum from the above equation has been fitted to the measured data using a non-linear least squares algorithm, the free parameters were a proportionality constant, a constant offset, the gap width Δ, an energy offset (due to a small instrumental offset in the bias voltage) and the temperature. In Fig. 4(a), the fitted spectrum is plotted together with the measured one and the residuum. We have found a gap size of 188 μeV close to previously measured values (≈175 − 190 μeV)[18,19] and a temperature of ≈140 mK. This value constitutes an upper limit for the real electronic temperature. The preparation of the tip on a gold crystal likely leads to a thin gold layer on the tip apex. Though this gold layer would become superconducting due to the proximity effect,[48] this would introduce a finite density of states in the gap and reduce the height of the coherence peaks – potentially leading to a higher apparent electronic temperature. It should also be noted that spectra vary considerably for different tips; depending on the tip condition, sometimes no superconducting gap is observed at all. The difference between the temperature of the STM head ($T_{STM} \approx 30$ mK) and the electronic temperature indicates that RF noise still leads to a non-negligible broadening of the tunneling spectrum despite careful filtering of all signal lines at room temperature. Additional filtering at low temperature should allow us to improve our spectroscopic resolution significantly.[25] Our value is a bit lower than what has been obtained (280 mK with a Al sample) for the UHV-compatible setup recently presented by Stroscio and co-workers.[49]

In Fig. 4(b), we display the dI/dV spectra measured as a function of magnetic field with a lock-in modulation of 20 μV. The superconducting gap with coherence peaks at energies ± 170 μV survives up to a magnetic field between 27.5 mT and 30 mT, which is almost three times higher than the critical field of bulk Al (≈10 mT). This increase in magnetic field has been observed in previous STM experiments with aluminum and lead tips.[19] This may occur due to the tip apex having a smaller size than the coherence length, where the superconductivity can survive up to magnetic fields higher than the critical field of the bulk material.[50]

We have also measured the superconducting gap with lock-in modulation applied in the range of 5–50 μV, as presented in Fig. 4(c). It is clearly visible that higher lock-in modulation broadens the coherence peaks and affects the shape of the superconducting gap. Calculated spectra according to Eqs. (2)–(4) are shown in Fig. 4(d) and compared well to the measured ones.

In conclusion, we have demonstrated successful operation of a dilution-refrigerator based SI-STM with *in situ* sample exchange and a base temperature below 10 mK.

ACKNOWLEDGMENTS

U.R.S acknowledges support by the Alexander-von-Humbold foundation and S.C.W acknowledges support by SPP1458 of the Deutsche Forschungsgemeinschaft (DFG).

[1] G. R. Stewart, Rev. Mod. Phys. **56**, 755 (1984).
[2] A. J. Schofield, Nature **465**, 553 (2010); P. Coleman, *ibid.* **474**, 290 (2011).
[3] A. Damascelli, Z. Hussain, and Z.-X. Shen, Rev. Mod. Phys. **75**, 473 (2003).
[4] S. V. Borisenko, V. B. Zabolotnyy, D. V. Evtushinsky, T. K. Kim, I. V. Morozov, A. N. Yaresko, A. A. Kordyuk, G. Behr, A. Vasiliev, R. Follath, and B. Büchner, Phys. Rev. Lett. **105**, 067002 (2010).
[5] Ø. Fischer, M. Kugler, I. Maggio-Aprile, C. Berthod, and C. Renner, Rev. Mod. Phys. **79**, 353 (2007).
[6] H. Suderow, S. Vieira, J. D. Strand, S. Budko, and P. C. Canfield, Phys. Rev. B **69**, 060504(R) (2004).
[7] A. R. Schmidt, M. H. Hamidian, P. Wahl, F. Meier, A. V. Balatsky, J. D. Garrett, T. J. Williams, G. M. Luke, and J. C. Davis, Nature **465**, 570 (2010).
[8] S. Ernst, S. Kirchner, C. Krellner, C. Geibel, G. Zwicknagl, F. Steglich and S. Wirth, Nature **474**, 362 (2011).

[9]J. E. Hoffman, K. McElroy, D.-H. Lee, K. M. Lang, H. Eisaki, S. Uchida, and J. C. Davis, Science **297**, 1148 (2002); K. McElroy, R. W. Simmonds, J. E. Hoffman, D.-H. Lee, J. Orenstein, H. Eisaki, S. Uchida, and J. C. Davis, Nature **422**, 592 (2003).
[10]J. Lee, M. P. Allan, M. A. Wang, J. Farrell, S. A. Grigera, F. Baumberger, J. C. Davis, and A. P. Mackenzie, Nat. Phys. **5**, 800 (2009).
[11]T. Hanaguri, S. Niitaka, K. Kuroki, and H. Takagi, Science **328**, 474 (2010).
[12]T. Hanaguri, Y. Kohsaka, M. Ono, M. Maltseva, P. Coleman, I. Yamada, M. Azuma, M. Takano, K. Ohishi, and H. Takagi, Science **323**, 923 (2009).
[13]J. Singleton and C. Mielke, Contemp. Phys. **43**, 63 (2002).
[14]X.-L. Qi and S.-C. Zhang, Rev. Mod. Phys. **83**, 1057 (2011).
[15]C. J. Chen, *Introduction to Scanning Tunneling Microscopy*, 2nd ed. (Oxford University Press, New York, 2008).
[16]S. H. Pan, E. W. Hudson, and J. C. Davis, Rev. Sci. Instrum. **70**, 1459 (1999).
[17]M. Kugler, C. Renner, Ø. Fischer, V. Mikheev, and G. Batey, Rev. Sci. Instrum. **71**, 1475 (2000); L. Zhang, T. Miyamachi, T. Tomanic, R. Dehm, and W. Wulfhekel, *ibid.* **82**, 103702 (2011).
[18]C. Debuschewitz, F. Münstermann, V. Kunej, and E. Scheer, J. Low Temp. Phys. **147**, 525 (2007).
[19]J. G. Rodrigo, H. Suderow, and S. Vieira, Eur. Phys. J. B **40**, 483 (2004); I. Guillamón, H. Suderow, S. Vieira, and P. Rodière, Physica C **468**, 537 (2008).
[20]N. Moussy, H. Courtois, and B. Pannetier, Rev. Sci. Instrum. **72**, 128 (2001).
[21]M. Marz, G. Goll, and H. v. Löhneysen, Rev. Sci. Instrum. **81**, 045102 (2010).
[22]H. le Sueur and P. Joyez, Rev. Sci. Instrum. **77**, 123701 (2006).
[23]H. Kambara, T. Matsui, Y. Niimi, and H. Fukuyama, Rev. Sci. Instrum. **78**, 073703 (2007).
[24]Y. J. Song, A. F. Otte, V. Shvarts, Z. Zhao, Y. Kuk, S. R. Blankenship, A. Band, F. M. Hess, and J. A. Stroscio, Rev. Sci. Instrum. **81**, 121101 (2010).
[25]H. le Sueur and P. Joyez, Rev. Sci. Instrum. **77**, 115102 (2006).
[26]M. Tinkham, *Introduction to Superconductivity*, 2nd ed. (Dover Publications, New York, 2004).
[27]Modified Kelvinox 400MX by Oxford Instruments, Tubney Woods, Abingdon, Oxfordshire, United Kingdom.
[28]S. H. Pan, Piezoelectric motor, International Patent WO 93/19494, International Bureau, World Intellectual Property Organization.
[29]C. Wittneven, R. Dombrowski, S. H. Pan, and R. Wiesendanger, Rev. Sci. Instrum. **68**, 3806 (1997).
[30]S. White, U. R. Singh, and P. Wahl, Rev. Sci. Instrum. **82**, 113708 (2011).
[31]Piezo actuators (model P-121.03) have been bought from Physik Instrumente GmbH & Co. KG, Karlsruhe, Germany.
[32]According to calculations by Oxford Instruments for the magnet.
[33]J. E. Hoffman, Ph.D. dissertation (University of California, Berkeley, 2003).
[34]Passive dampers (model I-2000) from Newport Corporation, Irvine CA, USA.
[35]RF Filters (model 1221-001) from Spectrum Control Inc., Fairview, PA, USA.
[36]RuO_2 temperature sensors from Lake Shore Cryotronics, Inc., USA.
[37]See http://www.softdb.com for Soft dB Inc., Québec, Canada.
[38]P. Zahl, M. Bierkandt, S. Schröder, and A. Klust, Rev. Sci. Instrum. **74**, 1222 (2003).
[39]P. Zahl, T. Wagner, R. Möller, and A. Klust, J. Vac. Sci. Technol. B **28**, C4E39 (2010).
[40]Femto GmbH (model DLPCA-200), Berlin, Germany.
[41]B. Giambattista, A. Johnson, R. V. Coleman, B. Drake, and P. K. Hansma, Phys. Rev. B **37**, 2741 (1988).
[42]The calibration of the *z*-piezo has been obtained from the height of occasionally seen step edges on different types of single crystals.
[43]R. C. Dynes, V. Narayanamurti, and J. P. Garno, Phys. Rev. Lett. **41**, 1509 (1978).
[44]I. Guillamón, H. Suderow, S. Vieira, L. Cario, P. Diener, and P. Rodière, Phys. Rev. Lett. **101**, 166407 (2008).
[45]Au(111) crystal was bought from MaTecK GmbH, Jülich, Germany.
[46]J. Bardeen, Phys. Rev. Lett. **6**, 57–59 (1961).
[47]J. Klein, A. Léger, M. Belin, D. Défourneau, and M. J. L. Sangster, Phys. Rev. B **7**, 2336 (1973).
[48]A. K. Gupta, L. Crétinon, N. Moussy, B. Pannetier, and H. Courtois, Phys. Rev. B **69**, 104514 (2004).
[49]N. Levy, T. Zhang, J. Ha, F. Sharifi, A. A. Talin, Y. Kuk, and J. A. Stroscio, preprint arXiv:1211.0267 (2012).
[50]M. Poza, E. Bascones, J. G. Rodrigo, N. Agraït, S. Vieira, and F. Guinea, Phys. Rev. B **58**, 11173 (1998); J. G. Rodrigo, H. Suderow, S. Vieira, E. Bascones, and F. Guinea, J. Phys.: Condens. Matter **16** R1151–R1182 (2004); Y. Chen, M. M. Doria, and F. M. Peeters, Phys. Rev. B **77**, 054511 (2008).